Polymer and bioink mixed strategy for human 3D printed Hippocampus model development

Felipe Valle Fortes Rodrigues
PUCRS - Brain Institute
Gabriele Zanirati
PUCRS - Brain Institute
Isadora Ghilardi
PUCRS - Brain Institute
Allan Marinho
PUCRS - Brain Institute
Thuany Maraschin
PUCRS - School of Technology
Nara Regina Bastos
PUCRS - School of Technology
Carlos A. dos Santos
PUCRS - School of Technology
Vitória Pimentel
PUCRS - Scientific Initiation Program
Lia Siqueira
PUCRS - Scientific Initiation Program
Daniel Marinowic
PUCRS - Brain Institute
Jaderson Costa DaCosta (jcc@pucrs.br)
PUCRS - Brain Institute

Research Article

Keywords:

Posted Date: February 17th, 2022

DOI: https://doi.org/10.21203/rs.3.rs-1307154/v1

Abstract

Science development can be directly correlated with the models and technologies applied to best simulate the analyzed environment in relation to the clinical reality to be studied and treated. 3D printers and bioinks enable the information acquisition from a clinical imaging environment and replicate it in an experimental one, such as cultured cells, with individual anatomical fidelity and control of cell layers, which mimic real tissue. Neuronal tissue greatly benefits from this approach because it´s a tissue hard to get samples, controls and with limitations in current cell culture monolayer models. Our results demonstrate the development of a model of human hippocampus with anatomical fidelity from magnetic resonance, printed with 3D technology in polylactic acid (PLA) polymer and brain decellularized tissue bioink. Therefore, we performed a screening aiming to determine the best materials. We performed hydrophobicity, surface morphology, cell viability, direct and indirect adhesion assays in the polymers, resulting in PLA among the best performing materials. Then we demonstrated a 3D model to comprehend hippocampus anatomy and histological complexity. Our results combine different expertise in the development of a model with the potential to enhance the study and application of therapeutic strategies regarding hippocampus pathologies.

Introduction

Neurodegenerative diseases are defined by impairment of neuronal network function. Such loss can be reflected in connectivity, individual cell integrity or even in the protection of the myelin sheath (1, 2). Probably one impacting factor in the incidence and prevalence of neurodegenerative pathologies is time and, as demonstrated in the 2015 United Nations report, the number of people over 60 years old tends will increase, highlighting the risk associated with these conditions. Pathologies (3, 4). The hippocampus is involved in the consolidation of memory and learning (1). In the clinic, there are a variety of diseases that affect the hippocampus, such as Alzheimer's and other neurodegenerative processes, like epilepsy and depression (5). Although it is a key structure in the injury resulting from numerous pathologies, clinical and laboratory practice still lacks models capable of simulating the arrangement of this structure, harboring difficulties regarding the study and development of biological interventions to these pathologies. The arrangement of monolayer cells, present in traditional culture, hinders the construction of models that mimic the cellular arrangement and physiological connectivity of the tissue. 3D printing, together with the use of biocompatible materials and hydrogels, contribute to the creation of structures with greater cytoarchitectural likelihood (6–9). These could allow a greater understanding of the intrinsic processes of the structure and, thus, help in the development of interventions for the pathological processes mentioned. Biomaterials are materials that aim to support and stimulate regeneration or replace functional tissue without causing rejection of the host, among them are biocompatible polymers and mesenchymal stem cells (MSC), in addition to their products such as exosomes (10–13). Hydrogels, in turn, are oxygen and nutrition permeable compounds, which allow cell migration and are widely used as tissue-specific extracellular matrix mimetizers, serving as scaffold for cell development (14)). Thus,

this work aims to build a 3D structural model of the hippocampus, through 3D printing using biocompatible polymers and cells in hydrogel medium.

Methods

Statistical analyses

All statistical analyses were performed using GraphPad Prism 8 software. Samples were analyzed through ANOVA with Tukey post hoc and $p < 0.05$ was considered statically significant.

Cell culture

Experiments were conducted with NIH-3T3 cell lineage, from the Cell and Tissue Technology Laboratory, Brain Institute (BraIns) at PUCRS. Cells were cultivated in the following maintenance medium: Dulbecco's Modified Eagle Medium (DMEM) supplemented with 10% fetal serum inactivated bovine (SFB), 100 U/mL penicillin/streptomycin and 100 µg/mL gentamicin, all purchased from the manufacturer GibcoTM (Gibco™, Life Technologies, California, USA).

Polymeric biomaterials preparation

Membranes of different film biomaterials were prepared in order to establish the most suitable for use in a 3D printed matrix. The biomaterials used were Policaprolactona (PCL), Poly Lactic-co-Glycolic Acid (PLGA), Polylactic acid (PLA) and Polypyrrole (PPY) in membrane. For the experiments, the membranes were used in the following configuration: PCL, blend of 70% of PCL and 30% of PLGA, PLA and PPY dispersed over the blend in the proportion of 10% m/m (15). For the experiments, film/membrane biomaterials were used. Briefly, the polymer matrices or their blends were prepared using the solvent evaporation methodology. The polymers were dispersed in chloroform and later placed in petri dishes. The solvent was evaporated for 24 h at room temperature (15). Blends containing conductive polymer were prepared from the addition of previously synthesized PPy nanofibers (10% w/w).

Contact angle

To evaluate film surfaces hydrophobicity, contact angle values were determined using a Phoenix 301 goniometer, SEO Company. The experiments were carried out with deionized water and determined soon after the contact of the drop with the material to be analyzed. Five drops of deionized water were applied and considered the medium value.

Infrared spectroscopy

The molecular structure of the materials produced was determined by Fourier transform infrared spectroscopy (FT-IR) in order to identify the functional groups present in the samples. The infrared (IR) measurement was performed through absorption spectrum, between 400–4000 cm − 1, in Perkin-Elmer spectrometer. It was used materials without exposure as control.

Cell viability

To verify the cytotoxic potential of the materials, MTT protocol was performed through the extraction method following the norms of ISO 10993-5. Briefly, for the production of conditioned medium, the biomaterials were exposed, in the proportion of $3cm^2$/mL, to the medium used for the cultivation of cells in their maintenance phase for a period of 24 hours, 72 hours and 7 days at culture conditions stated above. Cells were plated at a density of 5×10^4 cells per well in a 96-well plate and cultured for 24 hours in maintenance medium. Afterwards, cells were exposed to this conditioned medium, for 24 h and then incubated with the MTT solution at a concentration of 5 mg/mL for 2 hours. Absorbance was measured at 570 nm in SpectraMax equipment, molecular devices, San Jose, California.

Direct cell adhesion

To evaluate the adhesion potential, cells were cultured directly on $3cm^2$ of the biomaterials, at a density of 5×10^4 cells for 24 hours. Afterwards, the biomaterials were fixed with 4% paraformaldehyde for 15 minutes, washed and incubated with nuclear staining, 4',6'-diamino-2-phenyl-indole (DAPI), (10 µg/mL) for 15 minutes. Ten random fields were captured using a confocal microscope LSM 5 Exciter, Zeiss and the stained nuclei present on the matrices were quantified using Image Pro Plus® software version 6.0 (Media Cybernetics, Rockville, MD, USA)

Indirect cell adhesion

To assess the ability of the conditioned medium to influence cell adhesion, the biomaterials were exposed, at a rate of $3cm^2$/mL, to the same medium used for cell culture or to the conditioned medium for 24 hours, 72 hours and 7 days. Cell culture was performed in 2 moments, culture phase and adhesion phase, and then they were stained and the absorbance verified. Figure 1 demonstrates an schematic design of this experiment. In the culture phase, cells were cultured for 24 hours with maintenance or conditioned medium, at a density of 5×10^4 cells per well in 96-well plates, trypsinized and replated in the same concentrations to start adhesion phase. In the adhesion phase, the cells were exposed to the maintenance medium or to the conditioned medium for 4 hours. The cells were then washed with phosphate buffered saline, fixed with 4% paraformaldehyde for 15 minutes, washed with phosphate buffered saline, and incubated with cresyl violet for 15 min. After that, the absorbance was measured at 570 nm in the SpectraMax-M2 equipment, molecular devices, San Jose, California.

Magnetic Resonance (MR)

Structural magnetic resonance images were acquired on a General Electric (GE) 3 T Scanner with a 3D sagittal gradient acquisition by sequence echo (MP-RAGE). Repeat time of approximately 2300 ms, echo time of approximately 3 ms and inversion time of approximately 900 ms, and voxel dimensions were approximately 1.20 × 1.015 × 1.015 mm.

Scanning electron microscopy

The morphology and surface of the samples were analyzed using the scanning electron microscope (SEM), PHILIPS model XL30 with a resolution of 3.5 nm and a range of magnifications of 500 times for the films of polymeric biomaterials and up to 20.000 times for the hydrogels, with accelerating voltage of

20 kV. Samples were metallized with gold in the Sputter Coater equipment (Balzers SCD050). In the case of hydrogels with cells, samples were fixated with 4% paraformaldehyde for 24 hours, dehydrated with acetone prior to metallization protocol.

Polymer 3D printing

First for the hippocampal digital project model for the hippocampus, it was used Computer Aided Design (CAD) using the software CREO Parametric 3.0 in format *.stl for print. Data and measurements were extracted from the magnetic resonance imaging. For the 3D printing of the PLA mold, Fusion deposit modeling (FDM) technologies were used in Sethi S3 3D printer with simplify3D software. Print settings used as follows:

First layer:

• Nozzle diameter: 0.4 mm

• Layer height: 0.18 mm

• Extrusion multiplier: 0.95 mm (extrudes 0.95 mm of filament for every 1 mm the extruder travels)

• Temperatures:

Table = 60°C

Nozzle = 220°C

• Maximum speed (advance): 12 mm/s

Filling = 8.4 mm/s

Perimeter = 10.2 mm/s

• Cooling: 0% (0 PWM)

Other layers settings:

• Nozzle diameter: 0.4 mm

• Layer height: 0.12 mm

• Extrusion multiplier: 0.94 mm

• Temperatures:

Table = 60°C

Nozzle = 220°C

• Maximum speed (advance): 30 mm/s

Filling = 21 mm/s

Perimeter = 25.5 mm/s

• Cooling: 60% (153 PWM) – from the third layer

General Settings:

• Layers:

3 layers closed at the base (equivalent to 0.42 mm thickness)

5 layers closed on top (equivalent to 1 mm thickness)

4 layers (turns) closed on the perimeter (equivalent to 1.6 mm thickness

BioInk

For the hippocampus structural model it was used StandardInk™ and PlayInk™ from TissueLabs™ Sagl, Manno, Switzerland. For Methacrylate decellularized pig brain hydrogel it was used MatriXpectm GelMA also from TissueLabs™ Sagl, Manno, Switzerland. All bioinks were used following the manufacturer's instructions. The decellularized hydrogel composition by the manufacturer is as follows: 10% gelatin methacrylate; type I collagen < 1.5%; <0.3% elastin; 0.25% lithium trimethylbenzophosphinate; heparan sulfate < 0.2% chondroitin sulfate < 0.2% fibronectin < 0.1%.

BioInk 3D Model

3D printer was used through Repetier software, Hot-World GmbH & Co. In the software, the 5x5x1 mm cubic object was sliced with the Slic3r software (Slic3r, online open source company). The 22G extruder was placed 0.1 mm from the print platform. The object was printed at 0.07 mm^3/s, in three layers. For crosslinking, the object was left at 405 nm UV for 240 seconds, as recommended by the manufacturer. Parameters are below:

• Width of extrusion of external perimeters = 0.45 mm (0.06 mm^3/s)

• Width of perimeter extrusion = 0.50 mm (0.07 mm^3/s)

• Width of fill extrusion = 0.50 mm (0.07 mm^3/s)

• Width of solid fill extrusion = 0.50 mm (0.07 mm^3/s)

• Top fill extrusion width = 0.50 mm (0.07 mm^3/s)

Results

To evaluate the feasibility of an structural and compatible with cell culture 3D model of the human hippocampus, it was performed a screening of biomaterials to determine which material is the most effective to produce the mold, considering biological compatibility and production efficiency. The dimensions of the hippocampus were obtained from the volumetry of the human hippocampus from magnetic resonance imaging of the brain of an adult subject without hippocampal pathology; after digital mold design and 3D printing, we evaluated the structural reliability of the mold by magnetic resonance imaging. For the structuring of the hippocampus anatomical layers, we used 3D printing a bioink

Contact angle

To analyze the materials hydrophobicity, Fig. 2 shows the drop of deionized water on the material and it´s repulsion. The difference between the angles. PPY and PLA groups stood out with the highest contact angles (80,57 ± 0,76 and 71,73 ± 1,70, respectively), PPY being the highest and with no statistical difference between the PCL materials (63,08 ± 3,17) and 70/30 (63,81 ± 2,32). The PCL group had statistically smaller angles than the PLA and PPY groups. The 70/30 group had statistically smaller angles than the PLA and PPY groups. The PLA group had statistically lower angles than the PPY group.

Scanning Electron Microscopy of Polymeric Biomaterials

Figure 3 demonstrate the topographic difference between the materials, being controls materials not immersed in the medium and after being immersed in the period of production of the conditioned media and washed with deionized water. They were analyzed in the 24-hour, 72-hour and 7-day groups. The PCL and PLGA materials were flatter, while PLA and PPY proved to be rougher.

Infrared Spectroscopy

Figure 4 illustrate the infrared spectrum of the samples obtained from the chemical structure and demonstrate the infrared profile of all materials, being controls materials not immersed in the medium and after immersed in the period of production of the conditioned media 24 hours, 72 hours and 7 days. The samples were characterized by FTIR in transmittance mode in the range of 400–4000 cm-1 to identify the structural characteristics of the materials. None of the materials underwent changes in chemical bonds, during the analyzed period, as can be seen in the figures when the control spectrum is superimposed with the set after incubation in culture medium for 24, 72 hours and 7 days. The infrared spectrum of the blends with the addition of polypyrrole presents functional groups characteristic of blend due to pyrrole be 10% deposited over the blends.

Direct cell adhesion

Afterwards, we proceeded with the biological compatibility experiments. Figure 5 shows direct adhesion, cells were plated directly onto the biomaterials and cultured for 24 hours under normal conditions. Cells cultured in standard commercial culture plates were used as control. The 70/30 blend (106.12 ± 27.4)

was significantly more effective in allowing cell adhesion, demonstrating a statistical difference in relation to PCL groups (62.88 ± 15.1) and PPY (71.21 ± 9.2), but the same did not occur in relation to the PLA group (80.6 ± 18.6). The other groups showed no statistical difference between them.

Cytotoxicity assay

Regarding biomaterial toxicity potential, Fig. 5 demonstrates the results from the MTT assay performed using the conditioned media. Cells were cultured for 24 hours exposed to the conditioned medium, 24, 72 hours or 7 days, and then evaluated for relative viability in relation to the control. There were no significant differences in any time or group, except for PCL group (0.94 ± 0.41) using conditioned medium for 7 days.

Indirect adhesion

For indirect adhesion, two strategies were used: one thinking about the immediate effect of contact and the other about reversing this effect. For that, the cells were always cultivated in conditioned medium or exposed to the conditioned medium only during the adhesion period, in which case they were cultivated under normal conditions. Figure 7 demonstrate this results. As control, cells were always used under normal culture conditions. In experiments with PCL and blend materials, there were no statistical differences. In the experiments with the PLA material using the strategy of the experiment with the conditioned medium for 7 days, when the cells were placed in contact with this medium (DMEM-PLA; 87.20 ± 20), they showed a significant reduction in adhesion compared to the group always cultivated in conditioned medium (PLA-PLA; 143.4 ± 61.3). In the experiments with the PPY material, using the conditioned medium for 24 hours, the cells had significantly lower adhesion potential when cultured under normal conditions and when newly cultured with conditioned medium (DMEM-PPY; 127.84 ± 39, 1) comparing with cells grown in conditioned medium and in normal medium in the adhesion situation (PPY-DMEM; 168.24 ± 47.58). A reverse effect was observed, with the conditioned medium for 72 hours, significantly increasing the adhesion potential when cultivated under normal conditions and newly cultured with conditioned medium (DMEM-PPY; 128.83 ± 34.25), compared to those grown in conditioned medium and in normal medium in the adhesion situation (PPY-DMEM; 83.82 ± 23) and always in conditioned medium (PPY-PPY; 123.59 ± 55).

Polymer 3D mold printing

Figures 8 and 9 shows the acquisition of measurements obtained from magnetic resonance imaging of the brain regarding the hippocampus and the mold printing. Figure 8 demonstrate the axial (A, B and C) and coronal (D) planes. Figure 8 (F and G) shows the human hippocampus mold for 3D printing. Figure 9 (A and B) demonstrates the printed mold with the inlet and outlet on the top plate, to allow the mold to be associated with a pump to circulate the culture medium, aiming at the cultivation of cells inside. In Fig. 9 (C and D) we also verify the internal measurements that were in agreement with the measurements of the human hippocampus on magnetic resonance imaging.The magnetic resonance image of the impression

after printing (Fig. 9, C and D) resembles the image of the human hippocampus obtained in the sagittal section (Fig. 8, E).

3D hydrogel model

Figure 10 demonstrate the mold made with StandardInk™ and PlayInk™ bioinks, provided by the 3D printer manufacturer, It was built using smaller blocks with a lower support layer. This made it possible to use four different elements in its elaboration, consistent with the histological regions of the hippocampus. Figure 11 demonstrates cell adhesion by SEM.

Discussion

This work aims to enhance current knowledge regarding how to enable the use of emerging 3D technologies in the medical field (16) for the development of a model for research on neurodegenerative diseases; we chose the hippocampus for its relationship with memory processes (17) and its involvement in pathologies such as epilepsy (18) and Alzheimer's disease (19). Thus, the results analyze the acquisition of magnetic resonance images and the translation to the 3D printer using Fusion deposit modeling (FDM). After obtaining the computational model, we questioned which would be the most suitable material and from that, PLA, PCL, PLGA and PPY were elected as candidates. We worked with the membrane materials for the tests, using the blend of PCL and PLGA in the proportion of 70 to 30 percent respectively and the PPY was dispersed directly over the blend (15). In our contact angle results, PPY and PLA materials reached more hydrophobic contact angles but within the range of 70 to 80 brought by the literature. Zelzer and colleagues also demonstrated the survival, adhesion, and migration of hydrophobic hippocampal neurons within the spectrum of our results (20). The addition of arginine-glycine-aspartic acid (RGD motifs) amino acid sequences, which are essential for neuron cell adhesion (21), increases the hydrophobicity of the materials (22). This hypothetical mechanism could be related to PLA and PPY materials having higher contact angles and would benefit from using these materials. Another point that could be explored in future is that more hydrophobic materials may be related to the activation of astrocytes because the high contact angle can lead to modulation of the m1 and m2 profile (23, 24).

To verify the interaction of biomaterials with the surrounding environment, simulating in vitro how the presence of the biomaterial in a tissue could affect its surroundings, we performed indirect adhesion experiments. With the PPY group with conditioned medium for 24 hours, there was an increase in adhesion when it was returned to the conventional culture medium, demonstrating a possible reversal of some process that was affecting the cell. With the conditioned medium in 72 hours, the opposite occurred, a possible potentiation of the cell adhesion process in contact with the conditioned medium. With PLA, a possible potentiation of this process occurred when kept entirely in conditioned medium. Considering that we conducted an innovative experimental strategy between cultivation and the performance of the indirect adhesion experiment, aiming precisely to understand more carefully the changes in the adhesion process and possible reversal of the process, it is necessary to carry out complementary experiments to confirm this process and it´s mechanisms. From these results and considering the feasibility of PLA being printed directly on the 3D printer, we considered PLA as the most

suitable material for the construction of the mold due to the result in indirect adhesion can benefit the mold, did not present cytotoxicity and, statistically, was not inferior to other biomaterials in direct adhesion. We then printed based on the MRI measurements with space to be attached to an infusion pump, Jin et al. in an in vivo model of ischemia injury, demonstrated that the addition of artificial brain spinal fluid achieved good reparative potential (25).

The work from Mark and colleges. provides a solid model of the hippocampus (19). These models can be used to aid in medical diagnosis, histology (26), as a surgical targeting tool (27), and for teaching (16). However, to evaluate treatments and perhaps enable the practice of precision medicine, it is necessary to build scaffolds that allow cellularization, stablishing parameters that can be controlled and treated in addition to the patient's anatomy.

Our next questions were related to tissue histology and cell integration with respect to brain tissue and conducted 3D printing using hydrogels was the answer to these questions (28). Decellularized tissue hydrogels can bring great benefit due to the maintenance of extracellular matrix elements and biochemical guides that support the processes of cell growth, orientation and differentiation (29). In addition, the similarity of mechanical characteristics can also benefit populations of the nervous system. Leipzig et al. demonstrated that stiffness closer to that of brain tissue benefits the differentiation of neurospheres into neurons and myelination from oligodendrocytes (30). Crapo and colleagues also demonstrated that in addition to differentiation, neurons cultured in decellularized brain bioinks showed more projections than in bioinks from other tissues (31).

Conclusion

Our material selection of PLA that did not present cytotoxicity and, statistically, was not inferior to other biomaterials in direct adhesion, adds feasibility to the printing process because with PLA, the production of the negative mold can be done directly from the 3d software. The construction of the mold with bioink in small parts forming a whole, inspired by magnetic resonance voxels, made it possible for the mold to absorb the complexity of hippocampus regions. In addition, the model of construction of the hippocampus in hydrogel, which allow cell migration, serving as scaffold for cell development, contributes to the cellular layering, potentially mimicking real tissue cytoarchitecture. Taken together, our work can contribute to the 3D printing of a model of the human hippocampus using compatible biomaterial and bioink that allows simulating conditions in health or disease, seeking new therapeutic strategies.

Declarations

FUNDING:

Coordenação de Aperfeiçoamento de Pessoal de Nível Superior - Brazil (CAPES) – Finance Code 001, Conselho Nacional de Desenvolvimento Científico e Tecnológico (CNPq) and Pandurata Alimentos Ltda.

J.C.C. is a CNPq -1A researcher.

DECLARATION OF INTEREST

The authors declare no conflict of interest

References

1. Mitroshina EV, Yarkov RS, Mishchenko TA, Krut VG, Gavrish MS, Epifanova EA, et al. Brain-Derived Neurotrophic Factor (BDNF) Preserves the Functional Integrity of Neural Networks in the β-Amyloidopathy Model in vitro. Front Cell Dev Biol. 2020;8:582.
2. Ahmed RM, Devenney EM, Irish M, Ittner A, Naismith S, Ittner LM, et al. Neuronal network disintegration: common pathways linking neurodegenerative diseases. J Neurol Neurosurg Psychiatry. 2016;87(11):1234–41.
3. Heemels MT. Neurodegenerative diseases. Nature. 2016;539(7628):179.
4. Nations U. World Population Ageing 2015: United Nations; 2017.
5. Moodley KK, Chan D. The hippocampus in neurodegenerative disease. Frontiers of neurology and neuroscience. 2014;34:95–108.
6. Thoma CR, Zimmermann M, Agarkova I, Kelm JM, Krek W. 3D cell culture systems modeling tumor growth determinants in cancer target discovery. Advanced drug delivery reviews. 2014;69–70:29–41.
7. Amann A, Zwierzina M, Gamerith G, Bitsche M, Huber JM, Vogel GF, et al. Development of an innovative 3D cell culture system to study tumour–stroma interactions in non-small cell lung cancer cells. PloS one. 2014;9(3):e92511.
8. Puschmann TB, Zandén C, De Pablo Y, Kirchhoff F, Pekna M, Liu J, et al. Bioactive 3D cell culture system minimizes cellular stress and maintains the in vivo-like morphological complexity of astroglial cells. Glia. 2013;61(3):432–40.
9. Ma X, Qu X, Zhu W, Li YS, Yuan S, Zhang H, et al. Deterministically patterned biomimetic human iPSC-derived hepatic model via rapid 3D bioprinting. Proceedings of the National Academy of Sciences of the United States of America. 2016;113(8):2206–11.
10. Barker RA, Götz M, Parmar M. New approaches for brain repair-from rescue to reprogramming. Nature. 2018;557(7705):329–34.
11. Teixeira AI, Duckworth JK, Hermanson O. Getting the right stuff: controlling neural stem cell state and fate in vivo and in vitro with biomaterials. Cell Res. 2007;17(1):56–61.
12. Zhong Y, Bellamkonda RV. Biomaterials for the central nervous system. J R Soc Interface. 2008;5(26):957–75.
13. Oliveira EP, Silva-Correia J, Reis RL, Oliveira JM. Biomaterials Developments for Brain Tissue Engineering. Advances in experimental medicine and biology. 2018;1078:323 – 46.

14. Peppas NA, Sahlin JJ. Hydrogels as mucoadhesive and bioadhesive materials: a review. Biomaterials. 1996;17(16):1553–61.
15. Alvim Valente C, Cesar Chagastelles P, Fontana Nicoletti N, Ramos Garcez G, Sgarioni B, Herrmann F, et al. Design and optimization of biocompatible polycaprolactone/poly (l-lactic-co-glycolic acid) scaffolds with and without microgrooves for tissue engineering applications. Journal of biomedical materials research Part A. 2018;106(6):1522–34.
16. Dho Y-S, Lee D, Ha T, Ji SY, Kim KM, Kang H, et al. Clinical application of patient-specific 3D printing brain tumor model production system for neurosurgery. Scientific reports. 2021;11(1):7005.
17. Lisman J, Buzsáki G, Eichenbaum H, Nadel L, Ranganath C, Redish AD. Viewpoints: how the hippocampus contributes to memory, navigation and cognition. Nature neuroscience. 2017;20(11):1434–47.
18. Zanirati G, Azevedo PN, Marinowic DR, Rodrigues F, de Oliveira Dias AC, Venturin GT, et al. Transplantation of bone marrow mononuclear cells modulates hippocampal expression of growth factors in chronically epileptic animals. CNS neuroscience & therapeutics. 2015;21(5):463–71.
19. Marks M, Alexander A, Matsumoto J, Matsumoto J, Morris J, Petersen R, et al. Creating three dimensional models of Alzheimer's disease. 3D printing in medicine. 2017;3(1):13.
20. Zelzer M, Alexander MR, Russell NA. Hippocampal cell response to substrates with surface chemistry gradients. Acta biomaterialia. 2011;7(12):4120–30.
21. Kafi MA, Cho H-Y, Choi J-W. Engineered peptide-based nanobiomaterials for electrochemical cell chip. Nano Convergence. 2016;3(1):17.
22. Zelzer M, McNamara L, Scurr D, Alexander M, Dalby M, Ulijn R. Phosphatase responsive peptide surfaces. Journal of Materials Chemistry. 2012;22:12229–37.
23. Negrescu AM, Cimpean A. The State of the Art and Prospects for Osteoimmunomodulatory Biomaterials. 2021;14(6).
24. Khodadadei F, Liu AP, Harris CA. A high-resolution real-time quantification of astrocyte cytokine secretion under shear stress for investigating hydrocephalus shunt failure. Communications Biology. 2021;4(1):387.
25. Jin K, Mao X, Xie L, Galvan V, Lai B, Wang Y, et al. Transplantation of human neural precursor cells in Matrigel scaffolding improves outcome from focal cerebral ischemia after delayed postischemic treatment in rats. Journal of cerebral blood flow and metabolism: official journal of the International Society of Cerebral Blood Flow and Metabolism. 2010;30(3):534–44.
26. Au - Luciano NJ, Au - Sati P, Au - Nair G, Au - Guy JR, Au - Ha S-K, Au - Absinta M, et al. Utilizing 3D Printing Technology to Merge MRI with Histology: A Protocol for Brain Sectioning. JoVE. 2016(118):e54780.
27. Martín-Noguerol T, Paulano-Godino F, Riascos RF, Calabia-Del-Campo J, Márquez-Rivas J, Luna A. Hybrid computed tomography and magnetic resonance imaging 3D printed models for neurosurgery planning. Annals of translational medicine. 2019;7(22):684.

28. Mobaraki M, Ghaffari M, Yazdanpanah A, Luo Y, Mills DK. Bioinks and bioprinting: A focused review. Bioprinting. 2020;18:e00080.
29. Faust A, Kandakatla A, van der Merwe Y, Ren T, Huleihel L, Hussey G, et al. Urinary bladder extracellular matrix hydrogels and matrix-bound vesicles differentially regulate central nervous system neuron viability and axon growth and branching. Journal of biomaterials applications. 2017;31:088532821769806.
30. Leipzig ND, Shoichet MS. The effect of substrate stiffness on adult neural stem cell behavior. Biomaterials. 2009;30(36):6867–78.
31. Crapo PM, Tottey S, Slivka PF, Badylak SF. Effects of biologic scaffolds on human stem cells and implications for CNS tissue engineering. Tissue engineering Part A. 2014;20(1–2):313–23.

Figures

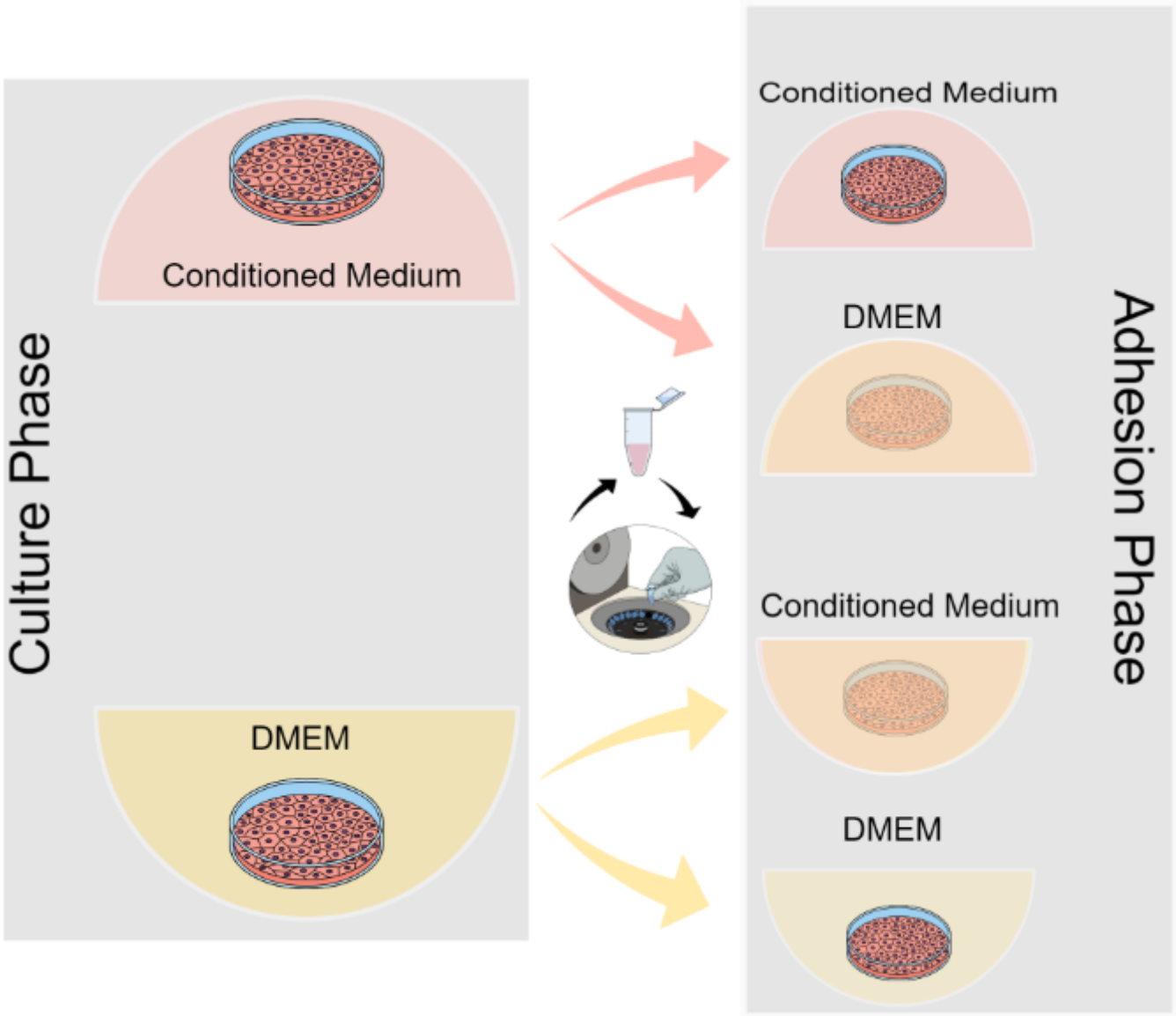

Figure 1

Demonstration of the indirect adhesion experiment. Initially the cells were cultured (“Culture phase”) in conditioned medium or under normal culture conditions (represented as DMEM). After the cells are placed to carry out the adhesion process exposed to normal conditions or to conditioned medium. Source: author.

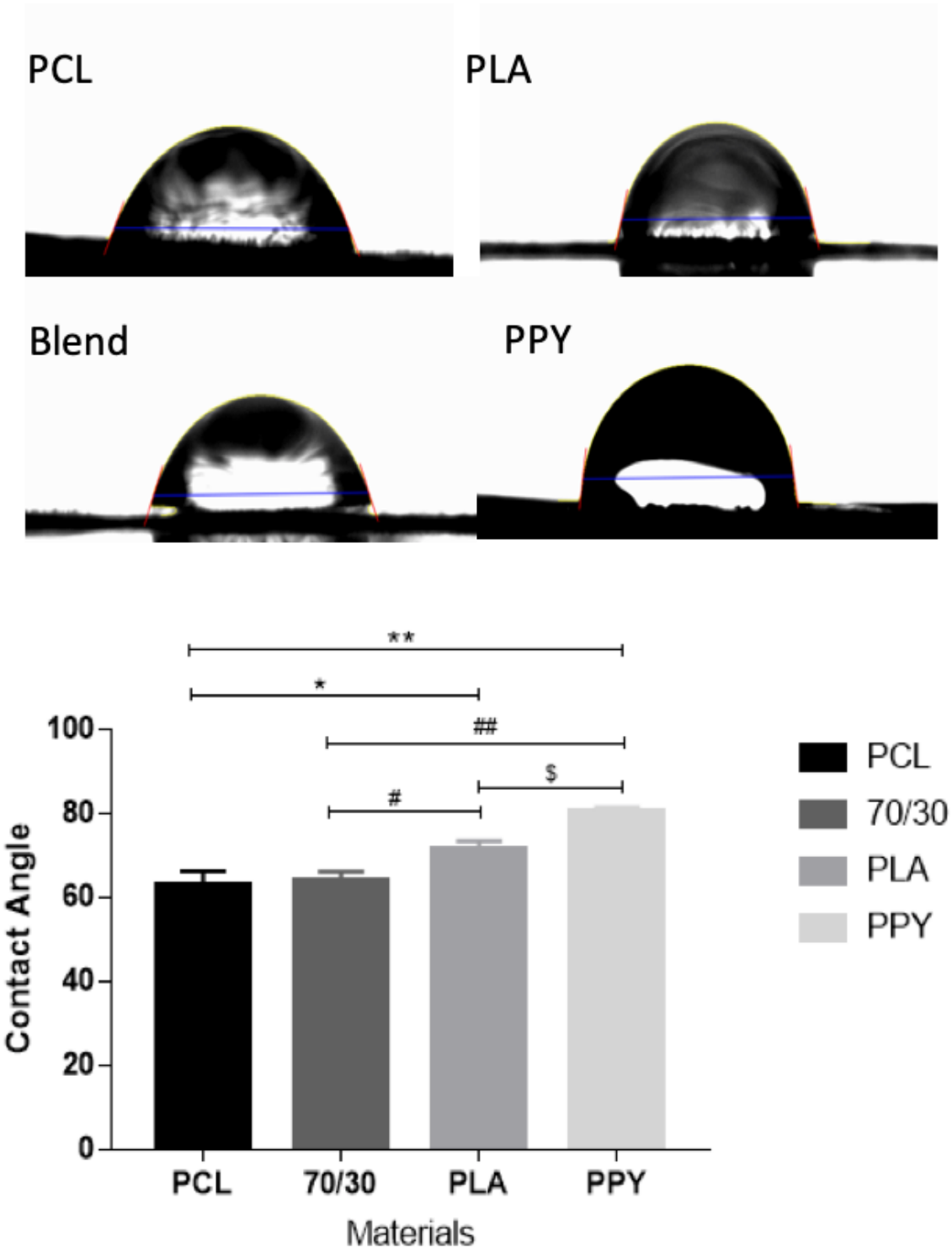

Figure 2

Demonstration of the contact angle. Analysis of the contact angle of biomaterials (angle ± SD, $p<0.05$); * represents the statistical difference between the PCL and PLA group; ** represents the statistical difference between the PCL and PPY.

Figure 3

Scanning electron microscopy of the biomaterials demonstrating the surface behavior over the period for the production of the conditioned medium, 24 and 72 hours and 7 days. As control it was used the materials without incubation.

Figure 4

Infrared spectrum of the PCL biomaterial. Left column represents control and right column the overlap with the set after incubation in culture medium for 24, 72 hours and 7 days

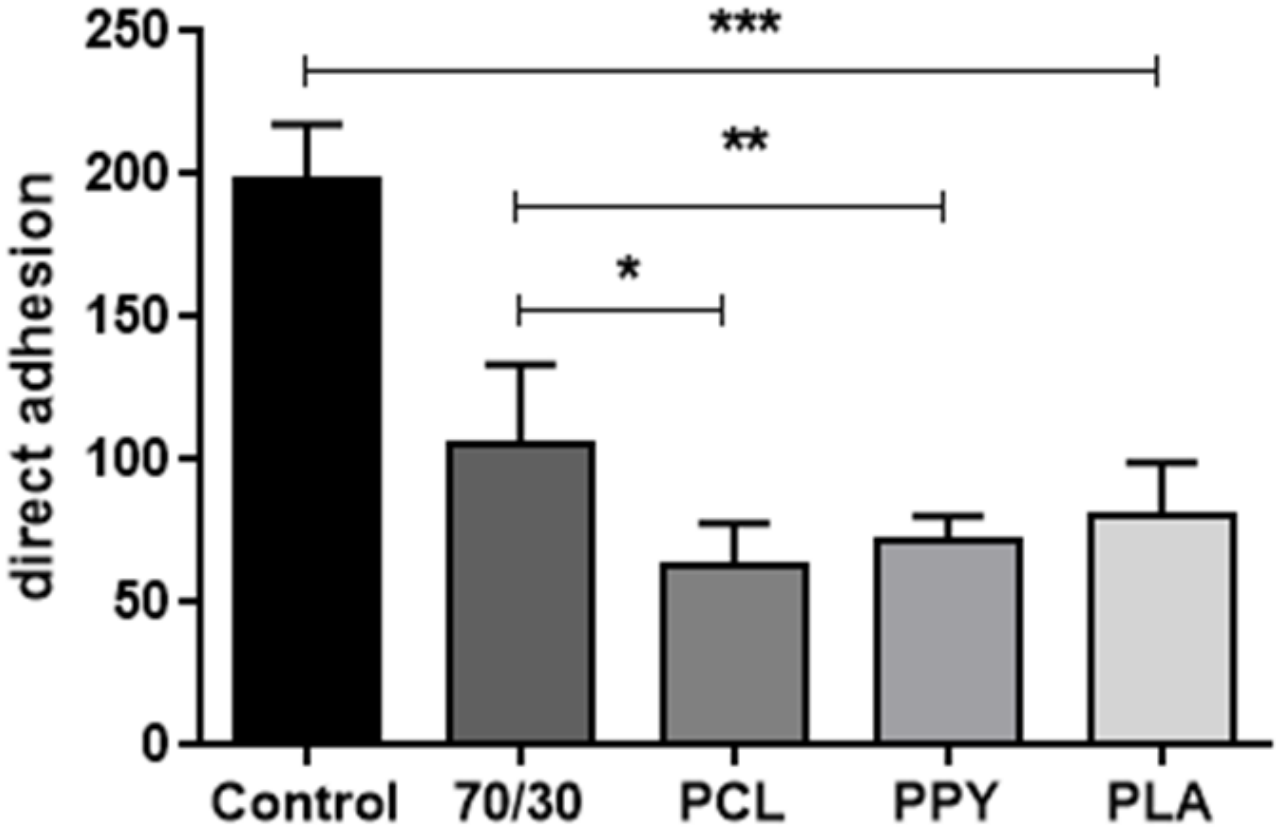

Figure 5

Analysis of direct adhesion on biomaterials (Count number± SD, $p<0.05$); * represents the statistical difference between the 70/30 group and PCL; ** represents the statistical difference between the 70/30 group and PPY; *** represents the statistical difference between all groups and the control group.

Figure 6

MTT viability assay using conditioned media for 24h, 72h and 7 days. * represents the statistical difference between PCL and the 3T3 control.

Figure 7

Indirect adhesion of cells (± SD, $p<0.05$). Initially grown in PPY or supplemented DMEM and allowed to adhere in conditioned medium or in supplemented DMEM. @represents the statistical difference between the DMEM-PLA group and PLA-PLA; * represents the statistical difference between the DMEM-PPY group and PPY-DMEM; ** represents the statistical difference between DMEM-PPY group and PPY-DMEM; ## represents the statistical difference between DMEM-PPY group and PPY-PPY.

Figure 8

Demonstration of the hippocampus measurements from MRI. A,B and C demonstrate the hippocampus in the axial plane, D in the coronal plane and E in the sagittal plane. F and G demonstrate the mold developed with those measures.

Figure 9

Mold printed on PLA. A and B demonstrate mold printed in similarity with hippocampus measures. C and D demonstrate the MRI of the mold.

Figure 10

Execution of the proposed model of construction of the hippocampus in hydrogel regarding its histological regions, using artificial material. In white, underneath, a support structure. In yellow, the region of the dentate gyrus. In pink, the region of CA3 and CA4. In blue the region of CA 1 and CA 2.

Figure 11

SEM of cell in the hydrogel. In A, cells were bioimprinted and cultured for 24 hours before being fixed and SEM performed. B and C demonstrate cell adhesion to the hydrogel